Heliyon 9 (2023) e21845

Contents lists available at ScienceDirect

Heliyon

journal homepage: www.cell.com/heliyon

Multi-parameter cardiac magnetic resonance imaging detects anthracycline-induced cardiotoxicity in rabbits model

Yurou Hu [a,d], Peisong Ma [b], Lin Chen [a,d], Juan Liu [c], Yongning Shang [c,**], Wang Jian [a,d,*]

[a] Department of Radiology, Southwest Hospital, Army Medical University (Third Military Medical University), Chongqing, China
[b] Department of Radiology, The First Affiliated Hospital of Chongqing Medical University, Chongqing, China
[c] Department of Ultrasound, Southwest Hospital, Army Medical University (Third Military Medical University), Chongqing, China
[d] 7T Magnetic Resonance Imaging Translational Medical Center, Southwest Hospital, Army Medical University (Third Military Medical University), Chongqing, China

ARTICLE INFO

Keywords:
T1 and T2 mapping
CMR
Anthracycline-induced cardiotoxicity
Animal models

ABSTRACT

Background: Cardiac magnetic resonance (CMR) quantitative T1 and T2 mapping offers a non-invasive means to evaluate early cardiotoxicity changes. This study aimed to pinpoint the earliest CMR indicators of myocardial injury in Anthracycline-induced cardiotoxicity (AIC) and to elucidate the connections between these CMR indicators and associated pathological indicators.
Methods: A total of 34 rabbits were administered doxorubicin at a dosage of 1 mg/kg/weekly. The study incorporated six 3T CMR scan time points: baseline, and at intervals of four, six, eight, twelve, and sixteen weeks. Cine, T1 and T2 mapping sequences assessed the left ventricular ejection fraction (LVEF), native T1, extracellular volume fraction (ECV), and T2 values. Following each time point, three rabbits were sacrificed for histological analysis involving Hematoxylin and eosin (H&E), Masson, TUNEL, and microvascular density (MVD) stains. Spearman correlations and linear mixed model analysis served in the statistical analysis.
Results: Diverse degrees of alternation were recorded in LVEF, native T1, T2, and ECV over time. LVEF declined to 49.0 ± 2.6 % at 12 weeks from the baseline of 53.4 ± 3.2 %, $p < 0.001$. Native T1 values increase from the baseline (1396.5 ± 79.2 ms) until 8 weeks (1498.8 ± 95.4 ms, $p < 0.001$). T2 values increased from the baseline (36.6 ± 3.3 ms) within 4 weeks of initiation (37.5 ± 3.4, $p = 0.02$) and remained elevated through 16 weeks (42.8 ± 0.3, $p < 0.01$). ECV was elevated at 8 weeks (33.9 ± 3.8 %, $p = 0.005$) compared to the baseline (30.2 ± 2.5 %). By week 12, myocardial edema and increased CVF were apparent ($p = 0.04$ and $= 0.001$, respectively). The area under ROC curve for positive CMR presence and the gold standards were 0.87 (T2-ROC, 4 weeks) and 0.92 (LVEF&BNP-ROC, 12 weeks).
Conclusion: T1 and T2 mapping are effective tools for cardiotoxicity detection and monitoring. The prolongation of T2 value emerged as the most consistent and early-onset indicator.

* Corresponding author. Department of Radiology, Southwest Hospital, Army Medical University (Third Military Medical University), Chongqing, China, 7T Magnetic Resonance Imaging Translational Medical Center, Southwest Hospital, Army Medical University (Third Military Medical University), Chongqing, China.
** Corresponding author.
E-mail addresses: ynshang@aliyun.com (Y. Shang), wangjian@aifmri.com (W. Jian).

https://doi.org/10.1016/j.heliyon.2023.e21845
Received 18 May 2023; Received in revised form 29 October 2023; Accepted 30 October 2023
Available online 12 November 2023

1. Introduction

Anthracyclines serve as the cornerstone drugs in the domain of cancer chemotherapy, as widely documented [1]. Intriguingly, these drugs exhibit a cumulative dose-dependent cardiotoxicity. Despite rigorous dose modulation aimed to averting cardiotoxicity, the prevalence of anthracycline-induced heart failure (HF) is on the rise [2]. Evaluating the intricate balance between efficacious cancer treatment and the onset of chronic HF poses a substantial burden on patients, both physically and psychologically.

Despite extensive research, the exact mechanism of anthracycline-induced cardiotoxicity (AIC) remains elusive. The primary operative mechanism is presumed to be closely tied with DNA intercalation, topoisomer-II inhibition, apoptosis, and iron-dependent reactive oxygen species production, culminating in pervasive oxidative damage within cardiac myocytes [3,4]. These pathophysiological transformations are manifested histologically as cardiac apoptosis, edema, and interstitial fibrosis [5]. The development of non-invasive imaging methods capable of reflecting these histological changes would be of paramount significance for the early diagnosis and accurate evaluation of AIC. In addition, the body of evidence is insufficient regarding microcirculatory cardiotoxicity, particularly the toxic effects of Anthracyclines on myocardium and vessels. Cardiac magnetic resonance (CMR) is currently the gold standard for evaluating cardiac structure and function [6]. Multiparametric CMR algorithms can assess myocardial function, perfusion, and tissue characteristics simultaneously [7]. With the advent of novel CMR techniques, T1-mapping can be employed to quantify diffuse myocardial fibrosis, while T2-mapping has been also associated with myocardial edema [8]. Although previous animal pathological studies have demonstrated the cardiac impact of different cumulative doses of anthracyclines, a method to facilitate comprehensive and dynamic early imaging of AIC is lacking [5,9,10].

The primary objective of this study was to employ a rabbit model to identify the earliest CMR indicators that are indicative of myocardial injury in the context of AIC. Additionally, the study aimed to explore the relationship between these CMR indicators and their corresponding pathological indicators.

2. Methods

2.1. Study design

This animal study was approved by our University (AMUWEC20203003), involved the use of thirty-four rabbits. All rabbits were administered DOX (doxorubicin hydrochloride; APE × BIO Technology LLC, Houston, TX, USA) at a rate of 1.0 mg/kg weekly via an intravenous route the ear vein. The rabbits underwent CMR examinations prior to the drug administration, at the four-week mark following the initial doxorubicin administration, and at intervals of 2–4 weeks thereafter until the end of the experiment. CMR scans

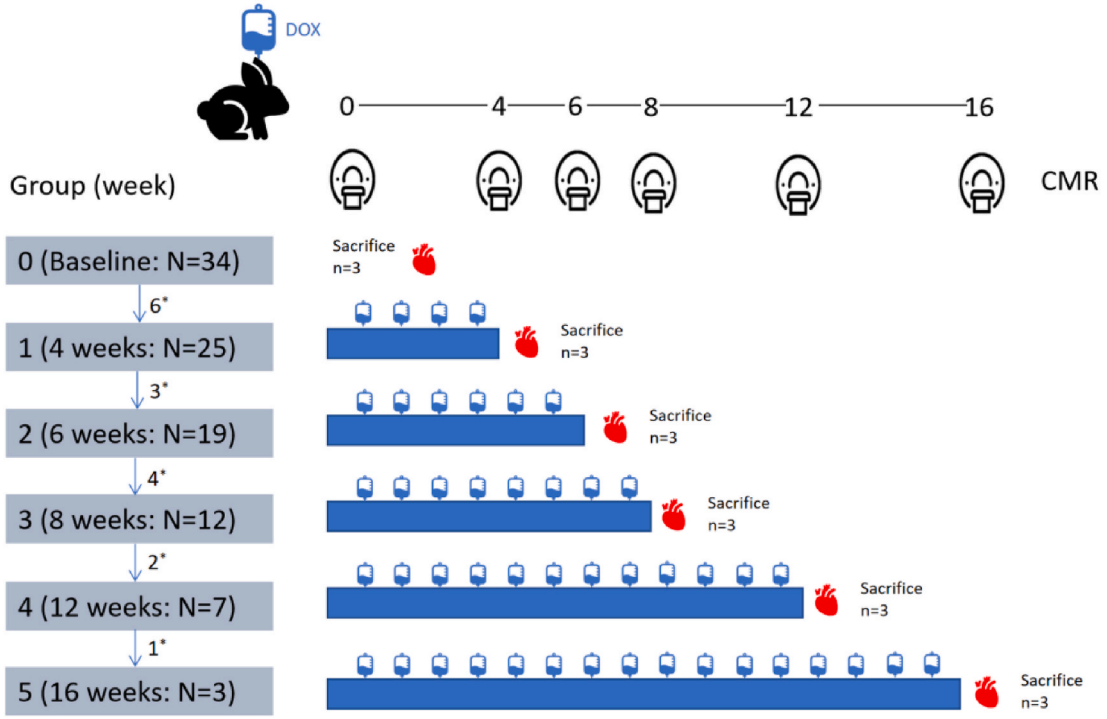

Fig. 1. Experimental design and the numbers of subjects in each group. Rabbits received intravenous doxorubicin (1 mg/kg/weekly). A total of 34 rabbits (total 100 time scan) were consecutively enrolled into six groups (group 0: baseline, group 1: 4 weeks, 2: 6 weeks, 3: 8 weeks, 4: 12 weeks, 5: 16 weeks). *: accidental death.

were executed at several time points: baseline, and at four, six, eight, twelve, and sixteen weeks. Subsequently, every third subject was sacrificed post-CMR scan. Weekly survival records were meticulously maintained (Fig. 1). One radiologist with over a decade of experience in CMR performed the scans, while image analysis was conducted by two additional radiologists, each with more than ten years of experience. A professional statistics researcher performed the statistical analysis. This study was designed as a triple-blind investigation.

2.2. Doxorubicin administration procedure

This study adapted previously delineated methods while modified the dosage specifically for this study [11–13]. The rabbits were anesthetized with pentobarbital (30–40 mg/kg intra-muscular, Pentobarbital® 6 %, Ceva, France). A diluted solution of Dox (1 mg/kg) in 0.9 % saline was administered intravenously into the auricular vein of the rabbits. The drug administration was performed over a duration exceeding 20 min by intravenous infusion. Given that doxorubicin is a particularly genotoxic agent, and a few rabbits exhibited signs of depilation or exudation injury during the course of the study [14,15].

2.3. CMR protocol

The MRI examinations were performed on a 3-T system (Magnetom Trio, Siemens Healthineers, Erlangen, Germany), equipped with a commercially specific 8-channel rabbit cardiac coil (Siemens Healthineers, Erlangen, Germany). Image shimming and the center frequency adjustments were made to mitigate artifacts arising from off-resonance signals. The CMR protocol included cine imaging, along with standard T1 and T2 mapping. Electrocardiogram (ECG)-gated steady-state free precession pulse sequence (bSSFP) cine sequences were employed to acquire cine images in Left Ventricular (LV) short- and long-axis planes (TR/TE/flip angle = 3.2 ms/1.3 ms/35°, FOV = 153 × 122 mm, slice thickness = 4 mm, matrix = 122 × 124). Standard T1 mapping was acquired with a modified Look-Locker Inversion recovery (MOLLI) sequence in a 5-(20)-3 mode (FOV = 400 × 300 mm2, matrix = 256 × 166, TR/TE = 301.7/1.09 ms, and 6 mm slice thickness). Pre-contrast T1 mapping was acquired in the mid-ventricular short-axis slice. Thereafter, a dose of 0.2 mmol/kg gadolinium contrast (Dotarem, Guerbet, BP7400, F95943, Roissy CdG Cedex, France) was injected intravenously. Approximately 10 min post-injection, a post-contrast T1 mapping sequence was initiated at the same location as the pre-contrast T1 measurement. Quantitative myocardial T2 mapping employed a bSSFP sequence with three TEs (0 ms, 25 ms, 55 ms). T2 mapping utilized the same image planes as T1 mapping, but with an 8 mm slice thickness and a spatial resolution of 2.7 × 2.1 mm2. T1 and T2 maps were subsequently generated after motion correction was performed in the MOLLI sequence (Fig. 2).

2.4. Image analysis

CVI42 software (Circle Cardiovascular Imaging, Calgary, Alberta, Canada) was used to analyze the cardiac structure and function. The endocardial and epicardial borders were manually traced on short-axis cine images to determine the end-diastolic volume (EDV) and the end-systolic volume (ESV), stroke volume (SV), ejection fraction (EF), cardiac output (CO), and Mass.

The endocardium and epicardium on the short axis plane of the middle-left ventricle were manually delineated. A circular region of interest (ROI) was then selected within the LV cavity, consciously avoiding the papillary muscle. T2, native, and post-contrast T1 values of the LV and blood cavity were measured automatically. Further, the myocardial ECV was also calculated as follows:

$$\mathrm{ECV} = (1 - HCT)\frac{\frac{1}{\mathrm{T1myo\ post}} - \frac{1}{\mathrm{T1myo\ native}}}{\frac{1}{\mathrm{T1blood\ post}} - \frac{1}{\mathrm{T1blood\ native}}}$$

The hematocrit (HCT) uses the mean of all rabbit results with HCT values.

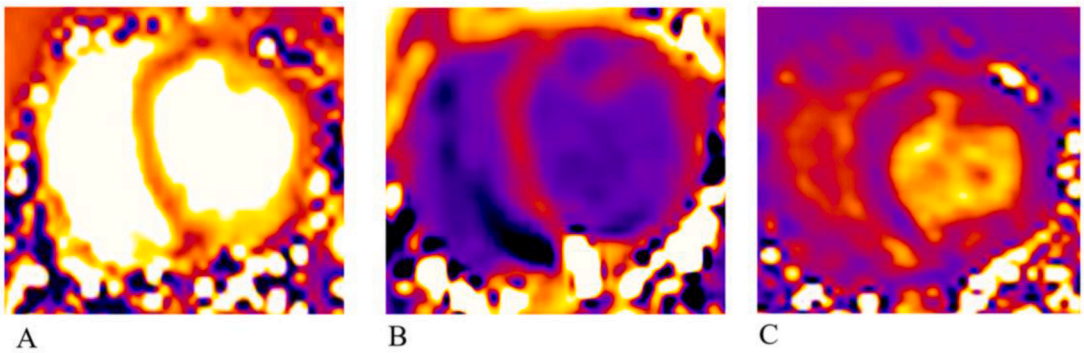

Fig. 2. Myocardial T1 and T2 mapping scan of a rabbit. (A) Diagram of Native T1 mapping data. (B) Diagram of Post-Contrast T1 mapping data. (C) Diagram of T2 mapping data.

2.5. Histological analysis

In each group, hearts tissue from three rabbits were preserved in 4 % formalin, and the mid-ventricular slice was embedded in paraffin. The levels of lactate dehydrogenase (LDH, Ruixinbo, Quanzhou, China), B-type Natriuretic Peptide (BNP, Jiangsu Jingmei Biological Technology Co., Ltd), lipid peroxidation (LPO, Jiangsu Jingmei Biological Technology Co., Ltd) and catalase (CAT, Ruixinbo, Quanzhou, China) were detected using ELISA. These slices were examined under a light microscope across six random selected visual fields (× 200). Hematoxylin and eosin (H&E) were utilized for assess histological morphology. Edema, typically correlated with myocardial injury, especially cell vacuolar change, was evaluated using the Billingham score (with the grading system as follows: 0 = no damage; 0.5 = not completely normal; 1, 1.5, 2, 2.5, and 3 = damage to 1–5%, 6–15 %, 16–25 %, 26–35 % and >35 % of all cells, respectively.) [16]. Interstitial fibrosis was detected through Masson's trichorome staining, and the collagen volume fraction (CVF = total collagen area/the total image area) was measured [17]. Tunel staining was performed to observed cell apoptosis by counting positive apoptotic cells [18]. Microvascular density (MVD) was calculated as the average number per field, based on the number of microvessels identified in the six fields post CD31 (Bioss, China) [19]. Quantitative analysis was performed using Image-Pro Plus 6.0 software (Media Cybernetics, Silver Spring, MD).

2.6. Statistical analysis

Results are presented as means ± standard deviations. The Kolmogorov-Smirnov test was performed to evaluate data normality distributions. For all comparisons, a $p < 0.05$ with two-tailed calculation was considered statistically significant.

Through restricted maximum likelihood, a linear mixed effects model was estimated. This model evaluated the time point at which a significant change occurred in the value of each variable (LVEF, myocardial native T1, ECV, myocardial T2) compared to the baseline group. Time was treated as a categorical variable in the mixed model to assess longitudinal changes in measured variables, and equal covariance was assumed between all-time points.

Histological quantification results (myocardial injury score, CVF, apoptosis number, MVD) were analyzed using one-way analysis of variance (ANOVA) tests with the post-hoc Turkey's method for multiple comparisons. The Pearson correlation coefficient was used to calculate the linear correlation between the myocardial imaging index and histological results.

Receiver Operating Characteristic curve (ROC-AUC) was also calculated to evaluate the diagnostic performances of ECV, myocardial native T1, T2, LVEF, and their combinations. Post-modeling groups were assumed to be disease positive. Bland-Altman analysis was used to evaluate the inter- and intra-observer variability of LVEF, T1,T2 and ECV measurements. A Kaplan-Meier survival curve was generated to illustrate rabbits mortality over time. Data were analyzed using SPSS (version 25.0, Statistical Package for the Social Sciences, International Business Machines, Inc. Armonk, New York, USA) and GraphPad Prism software (version 8.0, GraphPad Software, Inc, La Jolla, California, USA).

3. Results

3.1. Physiological characteristics

During the whole study, the body weight and blood biochemical indexes of rabbits were shown in Table 1, and no significant changes were found.

3.2. CMR date

The results from our CMR examinations demonstrated stable LVEF values up to 12 weeks mark, with baseline and 12 weeks values at 53.4 ± 3.2 % and 49.0 ± 2.6 %, respectively. The lowest LVEF value was observed at 16 weeks (47.7 ± 0.8 %) ($p < 0.001$). Native T1 value, significantly elongated from the baseline measure of 1396.5 ± 79.2 ms, was registered at 4 weeks as 1469.4 ± 67.5 ms ($p = 0.010$). This value remained stable for the subsequent 6–8 weeks and reverted to the baseline measurement by the 12 weeks. When compared to the baseline value of 30.2 ± 2.5 %, the ECV value showed a significant increase at the 8 weeks mark, reaching 33.9 ± 3.8 % ($p = 0.005$). The ECV value then continued to progressively rise throughout the cycle. For myocardial T2 values, a significant extension was observed at 4 weeks (37.5 ± 3.4 ms, $p = 0.018$) when compared to the baseline measurement of 36.6 ± 3.3 ms. In

Table 1
Physiological data of all subjects.

	baseline	4 Weeks	6 Weeks	8 Weeks	12 Weeks	16 Weeks
	(n = 34)	(n = 25)	(n = 19)	(n = 12)	(n = 7)	(n = 3)
weight, kg	2.6 ± 0.2	2.4 ± 0.2	2.4 ± 0.3	2.5 ± 0.3	2.7 ± 0.2	2.8 ± 0.1
Hematocrit, %	31.6 ± 1.5	32.5 ± 1.7	30.5 ± 4.3	32.0 ± 0.7	32.0 ± 2.0	32.6 ± 2.7
lactate dehydrogenase, IU/L	13.5 ± 5.9	17.8 ± 6.4	18.1 ± 1.6	12.6 ± 2.1	17.8 ± 2.5	15.3 ± 5.3
B-type Natriuretic Peptide, pg/mL	684.4 ± 89.5	779.0 ± 44.5	758.1 ± 75.5	733.9 ± 30.8	737.6 ± 29.2	721.1 ± 85.8
lipid peroxidation, pg/mL	267.7 ± 22.9	261.8 ± 66.2	433.3 ± 184.6	282.7 ± 31.6	290.5 ± 62.5	304.5 ± 55.8
catalase, U/ml	36.5 ± 13.4	31.5 ± 8.6	23.5 ± 4.6	32.0 ± 5.7	32.6 ± 7.8	28.3 ± 14.7

summary, the 16 weeks mark was the point at which peak LVEF, ECV, and myocardial native T2 values were all observed. Native T1, however, displayed a temporary change, reverting to baseline levels at 12 weeks. The earliest changes were noted in myocardial native T1 and T2 values, followed by alternations in ECV and LVEF measurement (Table 2, Fig. 3).

3.3. Histologic date

The model involves a spectrum of histopathological characteristics, including vacuolar changes of cardiomyocytes, interstitial edema, fibrosis, a reduction in microvessel density, and an increase in apoptotic bodies. As the modelling period extended, the mean CVF at 12 (5.3 ± 0.5 %) and 16 (7.8 ± 1.1 %) weeks were considerably higher than the baseline (2.0 ± 0.2 %; $p = 0.001$ and < 0.001, respectively) (Fig. 4AandB). A significant difference in myocardial injury was noticeable after 12 weeks ($p = 0.036$). However, symptoms such as cardiomyocyte edema were evident from as early as 4 weeks, with myocardial cells showing enlargement and a cytoplasm that was highly porous and vacuolated (Fig. 4CandD). Notably, the MVD, as determined by the CD31 method, did not change significantly during the observation period (Table 2).

3.4. Consistency and correlation analysis

In the analysis of the correlation between CMR data and histopathological data, this study found that T2 values moderately correlated with the CVFs ($r = 0.50$; $p = 0.03$, Fig. 5B). Furthermore, the ECV strongly correlated with the CVFs ($r = 0.81$; $p < 0.001$, Fig. 5C), and edema showed a moderate correlation with the CVFs ($r = 0.59$; $p = 0.01$, Fig. 5G). There was no correlation between T1 values and CVFs ($r = 0.20$; $p = 0.45$, Fig. 5A). Meanwhile, myocardial native T1 and T2 exhibited a robust correlation with histological edema on ($r = 0.77$, $r = 0.75$; respectively; $p < 0.001$, Fig. 5DandE), ECV moderately correlated with edema on histology ($r = 0.51$; $p = 0.03$, Fig. 5F). Bland-Altman statistical summaries and ICC values for inter and intraobserver differences are shown in terms of LVEF, with a 0.4 ms bias (range: −3.6–4.3 ms) for the interobserver group and a 0.3 ms bias (range: −3.5–4.0 ms) for the intraobserver group (Fig. 6AandB). For T1, there was a −5.0 ms bias (range: −63.7 to 53.7 ms) for the interobserver group and a −3.4 ms bias (range: −39.3 to 32.6 ms) for the intraobserver group (Fig. 6CandD). For ECV, there was a 0.1 % bias (range: −5.2–5.4 %) for the interobserver group and a −0.2 % bias (range: −6.4 to 6.1 %) for the intraobserver group (Fig. 6EandF). For myocardial T2 values, there was a −0.4 ms bias (range: −4.6 to 3.8 ms) for the interobserver group and a −0.3 ms bias (range: −4.0 to 3.4 ms) for the intra-observer group (Fig. 6GandH)

In terms of mortality, Kaplan-Meier curves were analyzed in relation to LVEF, T1, T2, and ECV values. However, these factors showed no statistical significance.

3.5. Diagnostic value of multi-parameter CMR

Firstly, post-modeling rabbits (4 weeks) were identified as being disease positive, and a ROC curve was constructed. The ROC-AUC of the LVEF, myocardial native T1, ECV, and T2 were 0.71 (95%CI, 0.459–0.890, $p > 0.05$), 0.65 (95%CI, 0.397–0.847, $p > 0.05$), 0.85 (95 % CI, 0.619–0.972, $p < 0.001$), and 0.88 (95%CI, 0.644–0.980, $p = 0.001$), respectively. Moreover, the cutoff points of ECV and T2 are >32.0 %, >35.1 ms (Fig. 7A). In the subsequently analysis, when the presence of pathology results (12 weeks) was the criteria for disease positivity, the AUCs of the LVEF, myocardial native T1, ECV, and T2 were 0.92 (95 % CI, 0.706–0.995, $p < 0.001$), 0.58 (95 % CI, 0.333–0.796, $p > 0.05$), 0.86 (95 % CI, 0.624–0.794, $p < 0.001$), and 0.64 (95 % CI, 0.393–0.844, $p > 0.05$), respectively. Here, the cutoff points of LVEF and ECV are ≤50.1 %, >32.2 %. In this case, the cutoff points for LVEF and ECV were determined as ≤50.1 % and >32.2 %, respectively (Fig. 7B). Furthermore, we performed an ROC analysis of LVEF, myocardial native T1, ECV, and T2, each in combination with BNP, based on the second analysis. It was observed that the ROC-AUC values for the combined indicators LVEF&BNP, T1&BNP, ECV&BNP and T2&BNP were 0.92 (95%CI, 0.706–0.995, $p = 0.002$), 0.58 (95%CI, 0.333–0.796, $p = 0.17$), 0.87 (95 % CI, 0.640–0.979, $p = 0.02$), and 0.68 (95%CI, 0.430–0.871, $p = 0.11$), respectively (Fig. 7C).

Table 2
Cardiac magnetic resonance (CMR) and Histological data of all subjects.

	baseline	4 weeks	6 weeks	8 weeks	12 weeks	16 weeks
	(n = 34)	(n = 25)	(n = 19)	(n = 12)	(n = 7)	(n = 3)
CMR date						
LVEF, %	53.4 ± 3.2	52.3 ± 2.7	52.2 ± 2.1	51.9 ± 1.7	49.0 ± 2.6[a]	47.7 ± 0.8[a]
Myocardium Native T1 value, ms	1396.5 ± 79.2	1469.4 ± 67.5[a]	1480.2 ± 69.9[a]	1498.8 ± 95.4[a]	1460.6 ± 75.6	1445.3 ± 60.9
Myocardium T2 value, ms	36.6 ± 3.3	37.5 ± 3.4[a]	40.1 ± 2.5[a]	40.1 ± 1.9[a]	41.1 ± 1.7[a]	42.8 ± 0.3[a]
ECV, %	30.2 ± 2.5	31.8 ± 2.3	32.2 ± 3.5	33.9 ± 3.8[a]	34.2 ± 1.8[a]	36.5 ± 1.1[a]
Histological data						
Edema score	0.0 ± 0.0	0.8 ± 0.3	0.9 ± 0.4	1.2 ± 0.8	1.8 ± 1.0[a]	1.6 ± 0.4
CVF, %	2.0 ± 0.2	2.6 ± 0.8	2.6 ± 0.5	3.6 ± 0.6	5.3 ± 0.5[a]	7.8 ± 1.1[a]
MVD, number	19.0 ± 8.5	12.8 ± 4.2	12.5 ± 0.7	12.5 ± 4.7	7.3 ± 3.2	10.0 ± 4.4

LVEF:left ventricular ejection fraction; ECV:extracellular volume fraction.CVF:collagen volume fractions; MVD:Microvascular density.
[a] Indicated $p < 0.050$. All data are expressed as mean ± SD.

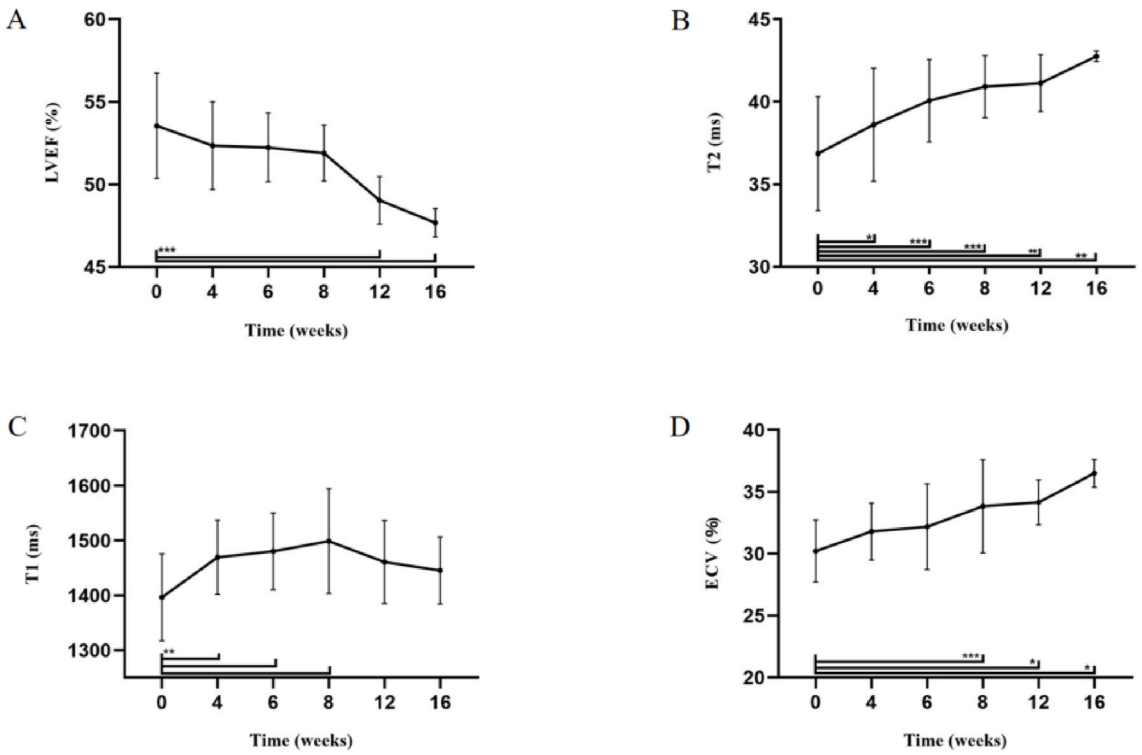

Fig. 3. Serial changes in animal model of Anthracycline Cardiotoxicity. (A) left ventricular ejection fraction (LVEF), (B) T2, (C) native T1 values, (D) extracellular volume (ECV). N= (0: 34, 4 weeks: 25, 6 weeks: 19, 8 weeks: 12, 12 weeks: 7, and 16 weeks: 3) *Indicated $p < 0.050$. **Indicated $p < 0.010$.***Indicated $p < 0.001$.

4. Discussion

The T1/T2-mapping multi-parametric CMR sequences are instrumental in providing quantitative information on changes in magnetic tissue characteristics. These changes effectively reflect alterations in composition of myocardial tissue. In this study, we observed that T1 and T2 values surged at the 4 weeks mark, a change associated with the histopathological manifestation of myocardial injury that became evident at 12 weeks. Subsequently, a notable change in ECV was detected after 8 weeks, a shift that correlated with an increase in myocardial collagen fibers apparent at 12 weeks. In assessing diagnostic efficacy at different intervals, the study found that T2 indicators reached optimal performance at 4 weeks, while ECV demonstrated greater statistical significance at 12 weeks. These findings indicated that CMR tissue characterization may have the potential to detect impending myocardial damage ahead of any observable deterioration in LV systolic function.

Currently, LVEF is utilized in clinical setting to diagnose cardiotoxicity. However, it is a broadly acknowledged that LVEF as a marker often indicates late-stage changes and does not detect the subclinical stage where cardiac function is still compensable [20]. Clinically, it is observed that once anthracycline-mediated deterioration of LVEF has occurred, the cardiac function seldom fully recovers [21]. Ideally, the earliest and most sensitive diagnosis should focus on cellular-level damage, a task well-suited for CMR tissue characterization. Previous studies have found that anthracyclines can cause an increase in ECV, but the relationship between T2 values and early cellular injury induced by anthracyclines has not been fully clarified [22,23]. This study demonstrates that anthracycline causes various histological changes over time, including cardiomyocyte edema and interstitial fibrosis. These changes are accompanied by a prolongation of T2 relaxation time, observed as early as 4 weeks post-administration. Similarly, native T1 relaxation time was found to increase within the same period. However, the T2 values measured through T2 mapping were not particularly effective in distinguishing the location of edema. This observation differs from Hong et al.'s study on pigs, where T2 changes preceded native T1, suggesting a higher likelihood of intracellular edema [9]. Interestingly, in our study, native T1 value returned to insignificance 12 weeks post-administration, while T2 continue to change throughout the 16-week period. We found no direct correlation between T1 and CVF. This may be because increases in native T1 values are mainly associated with changes in vacuoles, while T2 values consistently indicate intracellular edema [24,25]. Both T1 and T2 values have strong correlations with edema scores. Edema was found in our rabbit model, which aligns with the results of cross-sectional pathological studies in patients undergoing anthracycline treatment. Our study supplements the longitudinal studies of clinical patients through observed time-based changes.

Similar to edema, pathological clinical studies have reported myocardial fibrosis in patients undergoing anthracycline treatment. Previous clinical studies have suggested that myocardial fibrosis, caused by anthracycline, tends to diffuse. Late gadolinium enhancement (LGE) proves to be considerably less sensitive than ECV in detecting this. ECV reflects the extracellular matrix comprising

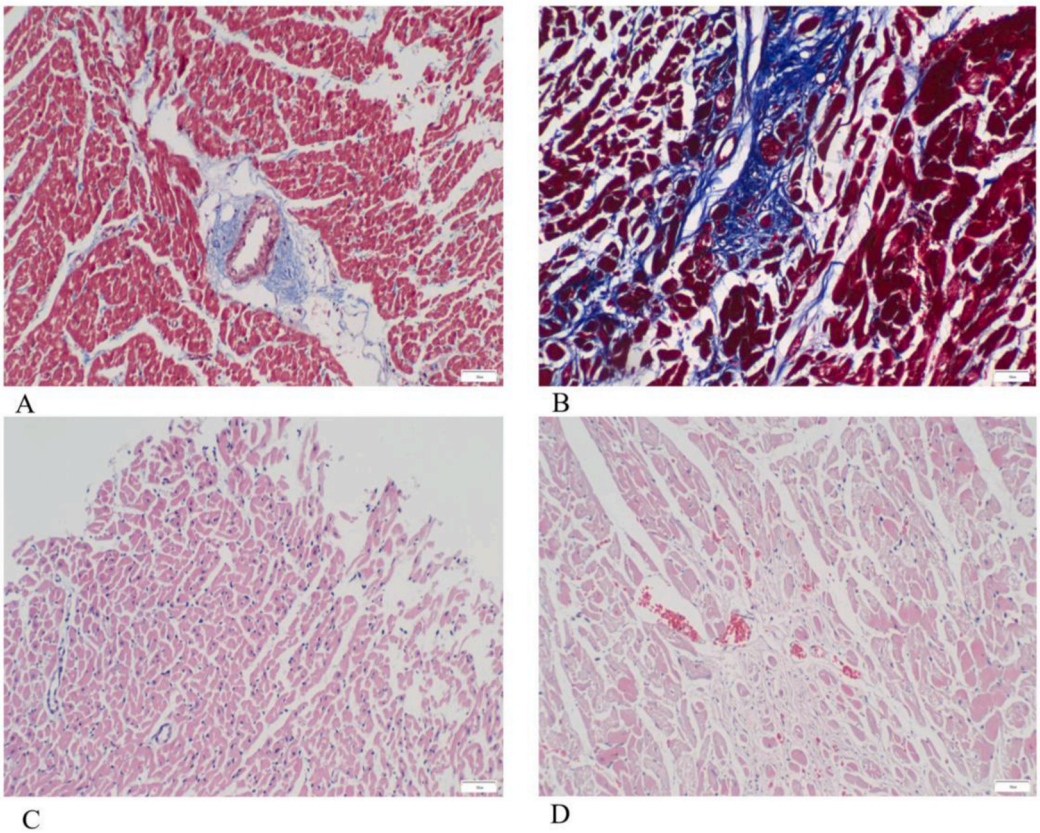

Fig. 4. Histological findings of myocardial injury and extracellular collagen deposition in the left ventricle myocardium. (A) Normal myocardium from a control subject, CVF = 2.03 %. (B) significant increase in collagen fibres was observed in the 12 weeks model CVF = 5.25 %. (C) Normal myocardium from a control subject. (D) Severe myocardial damage adjacent to the left ventricular is seen in the 12 weeks model, with widened myocardial interstitium, faint cell staining, and intracytoplasmic vacuolation. magnification, × 200.

the interstitial and intravascular space, which can quantify the extent of extracellular matrix expansion. Structural changes in myocardial remodelling, such as edema, fibrosis, or inflammation, are characteristic manifestations of cardiotoxicity caused by anthracyclines [26]. We supplemented the previous results of animal experiments on ECV. We observed a significant ECV increase 8 weeks post-administration and a substantial increase in CVF at 12 weeks. Notably, a strong correlation existed between ECV value and CVF, as well as between T2 value and myocardial edema, demonstrating a strongly linkage with CVF.

This study further assessed the role of conventional cardiac structure and function measurements in rabbits, especially focusing on the evolution of LVEF over time. Compared to other indicators observed at 4 or 8 weeks, changes in LVEF manifested later, only becoming discernible after 12 weeks. This reflects the gradual progression of chemotherapy-induced cardiotoxicity, which evolves from initial, subclinical cardiomyocyte injury to an asymptomatic decline in LVEF, culminating eventually in symptomatic heart failure. Moreover, this study also found that both T2 values and ECV were significantly superior in predicting myocardial toxicity, according to ROC curve analyses. Notably, T2 achieved the maximum AUC in the initial measurement following dosing. Furthermore, both ECV alone and in combination with BNP yielded excellent AUCs when pathological findings were used as the gold standard, underscoring their predictive potential in assessing myocardial toxicity.

In addition, our study did not identify any significant differences in LDH, LPO, CAT, and BNP levels within 16 weeks timeframe, nor did we observe a correlation between blood biochemical and CMR indicators. This could be attributed to the fact that, while blood biochemistry indicators hold independent predictive value, they are associated with cancer therapeutics–related cardiac dysfunction (CTRCD). However, the animal model has not yet met the criteria for CTRCD, suggesting that the blood biochemical parameters might be more indicative of hyperacute phase of myocardial injury (1–3 days) [27]. As for microvascular injury, our results were consistent with those from a study on coronary microcirculation in pigs, which suggests that the microvascular density did not undergo significantly changes during the duration of study [28].

Although using multi-parametric CMR as a routine method for monitoring myocardial damage caused by chemotherapeutic drugs may not be feasible, this study paves the way for future research directions. By examining a series of time-varying changes in CMR indices related to rabbit myocardial injury, combined with simultaneous pathological changes, CMR can be utilized as an effectively tool for non-invasive, qualitative, and quantitative assessment of myocardial damage. This approach provides a robust predictive capability that supports clinical preventive measures. Indeed, the potential for precisely timed interventions based on these analyses

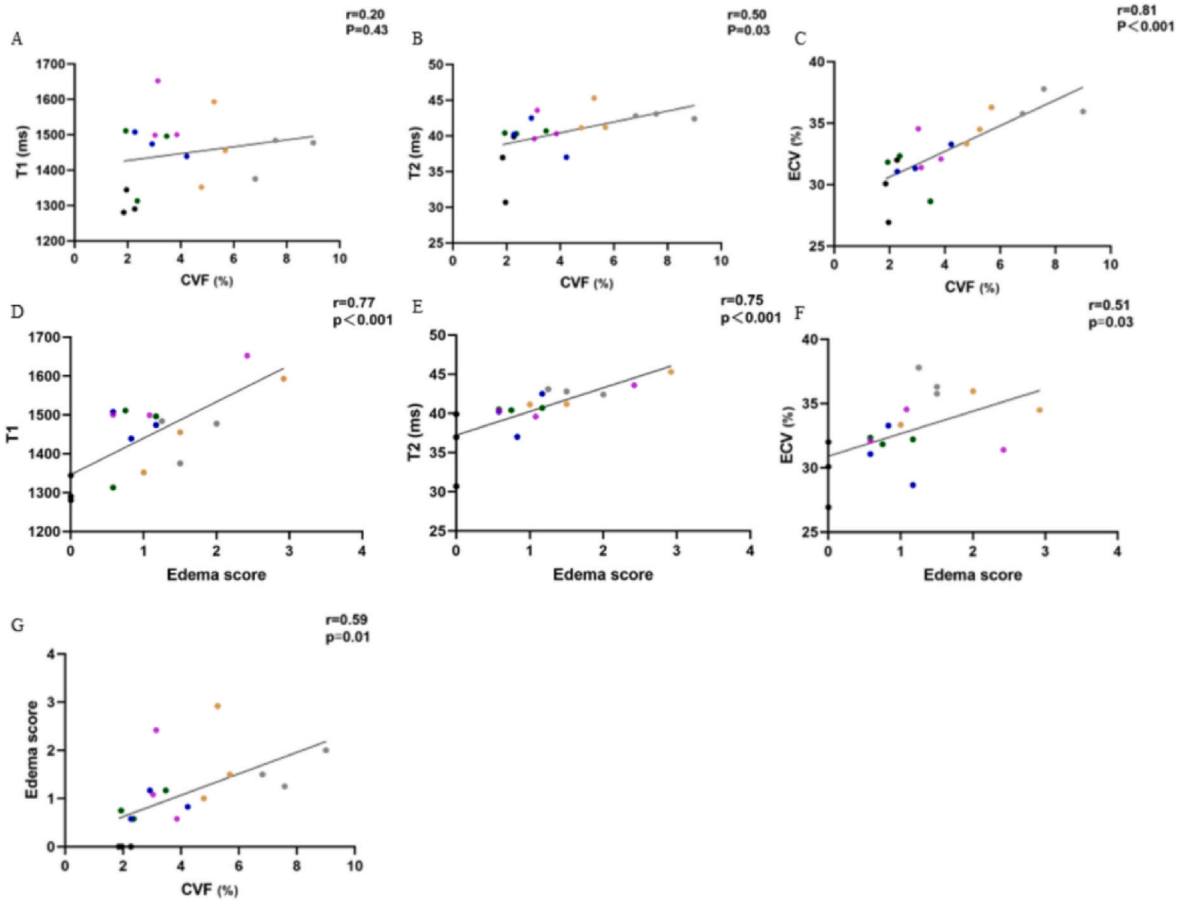

Fig. 5. Univariable regression analysis between native T1, T2 or ECV and histopathological findings. A. The nativeT1 value showed association with the CVFs change ($r = 0.20$; $p = 0.43$). B. The T2 showed moderately association with the CVFs change ($r = 0.50$; $p = 0.03$). C. The ECV value showed significant association with the CVFs change ($r = 0.81$; $p < 0.001$). D. The native T1 value showed significant association with the edema score change ($r = 0.77$; $p < 0.001$). E. The T2 value showed significant association with the edema score ($r = 0.75$; $p < 0.001$). F. The ECV value showed moderately association with the edema score change ($r = 0.51$; $p = 0.03$). G. Edema score showed moderately association with the CVFs change ($r = 0.59$; $p = 0.01$). Black = baseline; Green = 4weeks; Blue = 6weeks; Pink = 8weeks; Yellow = 12weeks; Gray = 16weeks. (For interpretation of the references to colour in this figure legend, the reader is referred to the Web version of this article.)

constitutes a substantial advancement in the management of chemotherapy-induced cardiac effects.

4.1. Limitations

This study has some limitations. First, we did not perform autopsy on rabbits that died accidently. Although survival analyses were performed on all rabbits, no significant CMR indicators were identified. Second, to validate the potential of T1 and T2 mapping in monitoring the cardiotoxicity of anthracyclines before dysfunction, larger histopathological sample sizes are required. Third, despite our efforts to emulate the actual clinical treatment cycle as closely as possible, it is important to recognize that in clinical settings, drugs are often not administered alone. The inclusion of a placebo treatment group and a drug withdrawal group is recommended for future studies, as it could provide more comprehensive and robust data regarding the cardiotoxicity and reversibility of anthracycline-induced effects.

5. Conclusion

This study found that myocardial T1 and T2 mapping could serve as a reliable and non-invasive method for detecting and monitoring cardiotoxicity. Of all the CMR markers investigated, the most consistent and early-onset indicator was found to be the prolongation of T2 value.

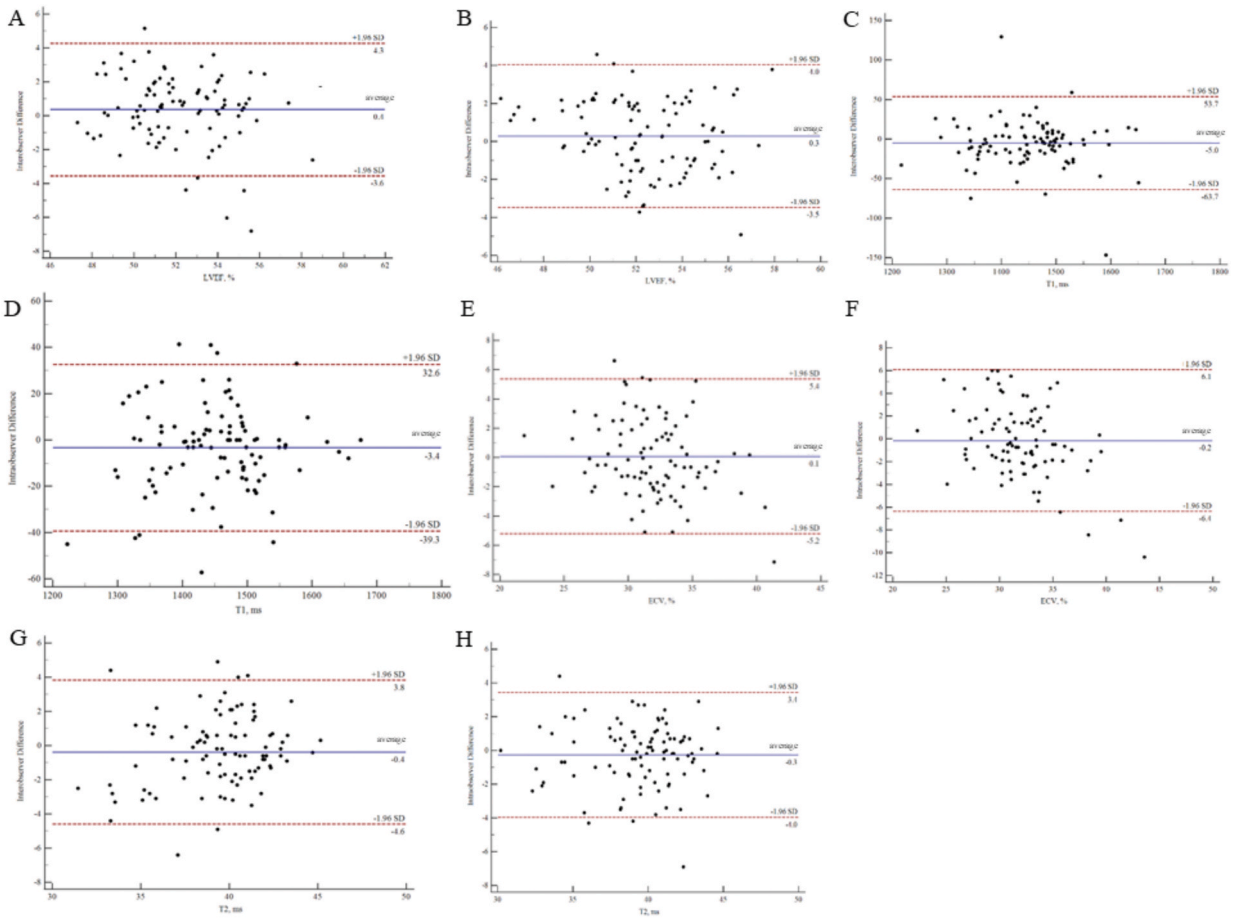

Fig. 6. Bland–Altman plots for inter- and intra-observer differences obtained for myocardial LVEF, T1, T2 values and ECV. (A, B): The inter- and intraobserver difference of LVEF values. (C, D): The inter- and intraobserver difference of T1values. (E, F): The inter- and intraobserver difference of ECV values. (G, H): The inter- and intraobserver difference of T2 values.

Ethics approval

The study was conducted according to the guidelines of.

National Research Council's Guide for the Care and Use of Laboratory Animals by Animals Ethics Committee of the Army Medical University, (AMUWEC20203003).

Data availability statement

The data that support the findings of this
study are available from the corresponding author upon request.

Funding

This work was funded by the National Natural Science Foundation of China (grant number 81971587), National InnovationTalent Promotion Program (4139Z2399), the Natural ScienceFoundation of Chongqing (grant number cstc2020jcyj-msxmX0399), and Chongqing postdoctoral Science Foundation (grant number CSTB2022BSXM-JCX0032).

CRediT authorship contribution statement

Yurou Hu: Conceptualization, Data curation, Formal analysis, Writing – original draft, Writing – review & editing. **Peisong Ma:** Data curation, Visualization, Formal analysis. **Lin Chen:** Methodology, Project administration. **Juan Liu:** Formal analysis, Project administration, Visualization. **Yongning Shang:** Conceptualization, Data curation, Funding acquisition, Investigation, Writing – review & editing. **Wang Jian:** Conceptualization, Funding acquisition, Investigation, Methodology, Resources, Writing – review &

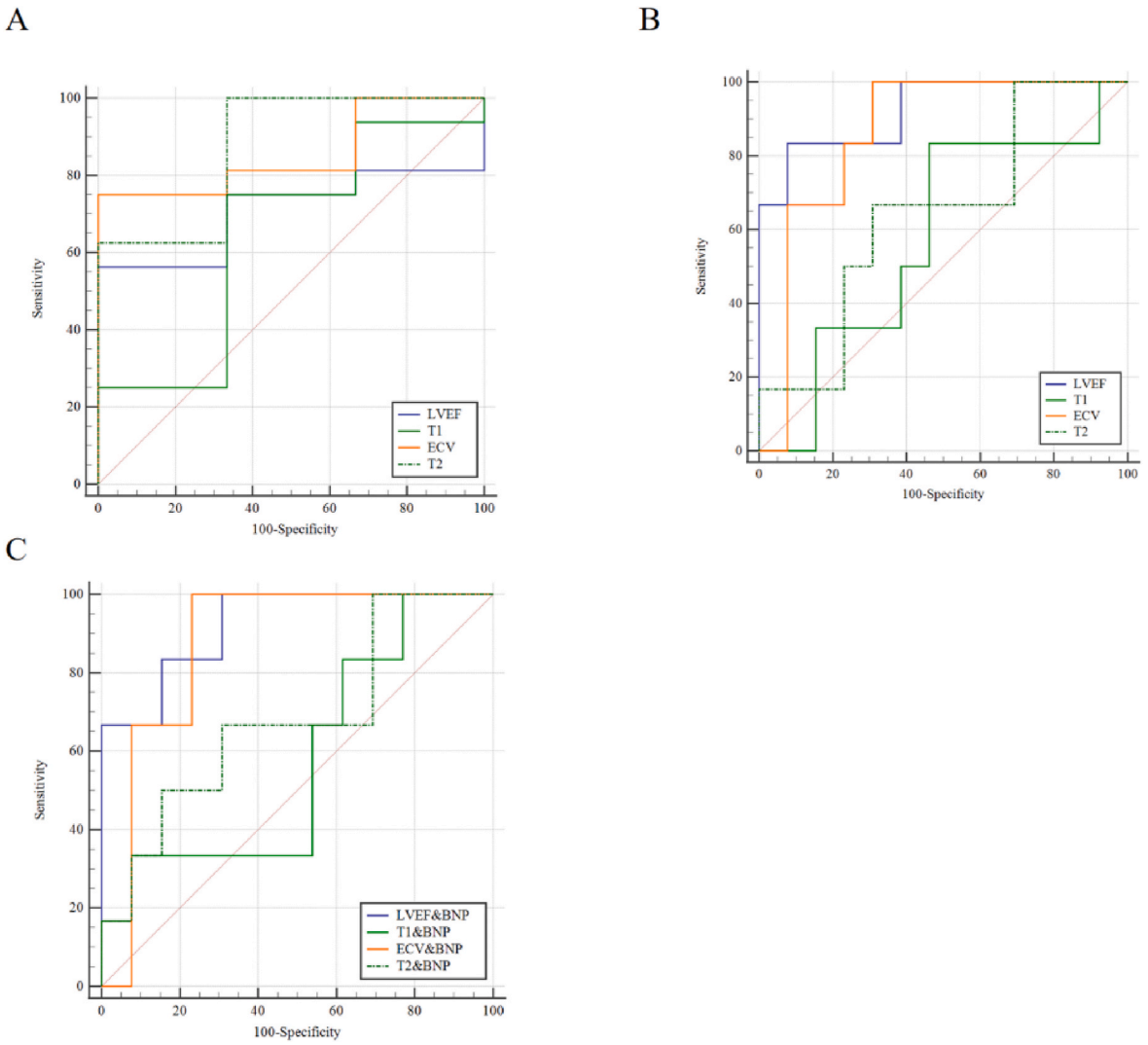

Fig. 7. Receiver operating characteristic (ROC) curves for diagnosis. (A) In the 4 weeks modelling subjects, the Areas under the ROC curves (AUCs) for the left ventricular ejection fraction (LVEF), native T1, extracellular volume (ECV), and T2 in post-modelling subjects were 0.71 (95%CI, 0.459–0.890, $p > 0.05$), 0.65 (95CI, 0.397–0.847, $p > 0.05$), 0.85 (95 % CI, 0.619–0.972, $p < 0.001$), and 0.88 (95%CI, 0.644–0.980, $p = 0.001$), respectively. (B) In the 12 weeks modelling subjects, the AUCs for the LVEF, native T1, ECV, and T2 were 0.923 (95 % CI, 0.706–0.995, $p < 0.001$), 0.58 (95 % CI, 0.333–0.796, $p > 0.05$), 0.86 (95 % CI, 0.624–0.794, $p < 0.001$), and 0.64 (95 % CI, 0.393–0.844, $p > 0.05$), respectively. (C) In the CMR date with BNP subjects, the AUCs for LVEF&BNP, T1&BNP, ECV&BNP and T2&BNP were 0.92 (95%CI, 0.706–0.995, $p = 0.002$), 0.58 (95%CI, 0.333–0.796, $p = 0.17$), 0.87 (95 % CI, 0.640–0.979, $p = 0.02$), and 0.68 (95%CI, 0.430–0.871, $p = 0.11$), respectively.

editing.

Declaration of competing interest

The authors declare that they have no known competing financial interests or personal relationships that could have appeared to influence the work reported in this paper.

References

[1] V.S. Hahn, D.J. Lenihan, B. Ky, Cancer therapy–induced cardiotoxicity: basic mechanisms and potential cardioprotective therapies, J. Am. Heart Assoc. 3 (2) (2014 Apr 22), e000665, https://doi.org/10.1161/JAHA.113.000665.

[2] Hani M. Babiker, Ali McBride, Michael Newton, M. Leigh, Boehmer, Adrienne Goeller Drucker, Mollie Gowan, et al., Cardiotoxic effects of chemotherapy: a review of both cytotoxic and molecular targeted oncology therapies and their effect on the cardiovascular system, Crit. Rev. Oncol. Hematol. 126 (2018) 186–200, https://doi.org/10.1016/j.critrevonc.2018.03.014.

[3] Giorgio Minotti, Pierantonio Menna, Emanuela Salvatorelli, Gaetano Cairo, Luca Gianni, Anthracyclines: molecular advances and pharmacologic developments in antitumor activity and cardiotoxicity, Pharmacol. Rev. 56 (2) (2004), https://doi.org/10.1124/pr.56.2.6, 185-229.

[4] Malgorzata Tokarska-Schlattner, Michael Zaugg, Christian Zuppinger, Theo Wallimann, Uwe Schlattner, New insights into doxorubicin-induced cardiotoxicity: the critical role of cellular energetics, J. Mol. Cell. Cardiol. 41 (3) (2006) 389–405, https://doi.org/10.1016/j.yjmcc.2006.06.009.

[5] Carolyn J. Park, Mary E. Branch, Sujethra Vasu, Giselle C. Meléndez, The role of cardiac MRI in animal models of cardiotoxicity: hopes and challenges, Journal of Cardiovascular Translational Research 13 (3) (2020) 367–376, https://doi.org/10.1007/s12265-020-09981-8.

[6] O'Quinn Rupal, Victor A. Ferrari, Ryan Daly, Greg Hundley, Lauren A. Baldassarre, Yuchi Han, et al., Cardiac magnetic resonance in cardio-oncology: advantages, importance of expediency, and considerations to navigate pre authorization, JACC (J. Am. Coll. Cardiol.): CardioOncology 3 (2) (2021) 191–200, https://doi.org/10.1016/j.jaccao.2021.04.011.

[7] S Jiji Ronny, Christopher M. Kramer, Michael Salerno, Non-invasive imaging and monitoring cardiotoxicity of cancer therapeutic drugs, J. Nucl. Cardiol. 19 (2) (2012) 377–388, https://doi.org/10.1007/s12350-012-9512-2.

[8] Riccardo Cau, Pierpaolo Bassareo, Valeria Cherchi, Vitanio Palmisano, S Suri Jasjit, Michele Porcu, et al., Early diagnosis of chemotherapy-induced cardiotoxicity by cardiac MRI, Eur. J. Radiol. 130 (2020), 109158 j.ejrad.2020.109158.

[9] Carlos Galán-Arriola, Manuel Lobo, Jean Paul Vílchez-Tschischke, López Gonzalo J, Antonio de Molina-Iracheta, Claudia Pérez-Martínez, et al., Serial magnetic resonance imaging to identify early stages of anthracycline-induced cardiotoxicity, J. Am. Coll. Cardiol. 73 (7) (2019) 779–791, j.jacc.2018.11.046.

[10] Heae Surng Park, Yoo Jin, Hong, Kyunghwa Han, Pan Ki Kim, Eunkyung An, Ji Yeon Lee, et al. Ultrahigh-field cardiovascular magnetic resonance T1 and T2 mapping for the assessment of anthracycline-induced cardiotoxicity in rat models: validation against histopathologic changes, J. Cardiovasc. Magn. Reson. 23 (1) (2021 Jun 17) 76, https://doi.org/10.1186/s12968-021-00767-8.

[11] K. Varsha, Sonawane, Umesh B. Mahajan, D Shinde Sachin, Subhajit Chatterjee, Sandip S Chaudhari 1, Harshada A. Bhangale, et al., A chemosensitizer drug: disulfiram prevents doxorubicin-induced cardiac dysfunction and oxidative stress in rats, Cardiovasc. Toxicol. 18 (5) (2018) 459–470, https://doi.org/10.1007/s12012-018-9458-y.

[12] Yoo Jin, Hong, Tai Kyung Kim, Donghyun Hong, Chul Hwan Park, Sae Jong Yoo, Mary Ellen Wickum, Hur Jin, et al., Myocardial characterization using dual energy CT in doxorubicin-induced DCM: comparison with CMR T1-mapping and histology in a rabbit model, JACC Cardiovasc Imaging 9 (7) (2016 Jul) 836–845, https://doi.org/10.1016/j.jcmg.2015.12.018.

[13] Jesús Talavera, Alejandro Giraldo, María Josefa Fernández-Del-Palacio, Obdulio García-Nicolás, Juan Seva, Gavin Brooks, et al., An upgrade on the rabbit model of anthracycline-induced cardiomyopathy: shorter protocol, reduced mortality, and higher incidence of overt dilated cardiomyopathy, BioMed Res. Int. 2015 (2015) 1–13, https://doi.org/10.1155/2015/465342.

[14] Karin Jordan, Timo Behlendorf, Franziska Mueller, Hans-Joachim Schmoll Anthracycline extravasation injuries: management with dexrazoxane, Therapeut. Clin. Risk Manag. 5 (2) (2009 Apr) 361–366, https://doi.org/10.2147/tcrm.s3694.

[15] Brian B. Hasinoff, Daywin Patel, Xing Wu, A QSAR study that compares the ability of bisdioxopiperazine analogs of the doxorubicin cardioprotective agent dexrazoxane (ICRF-187) to protect myocytes with DNA topoisomerase II inhibition, Toxicol. Appl. Pharmacol. 399 (2020), 115038, https://doi.org/10.1016/j.taap.2020.115038.

[16] Soichiro Ikeda, Shouji Matsushima, Kosuke Okabe, Masataka Ikeda, Akihito Ishikita, Tomonori Tadokoro, Nobuyuki Enzan, et al., Blockade of L-type Ca2+ channel attenuates doxorubicin-induced cardiomyopathy via suppression of CaMKII-NF-κB pathway, Sci. Rep. 9 (1) (2019 Jul 8) 9850, https://doi.org/10.1038/s41598-019-46367-6.

[17] Elias Daud, Offir Ertracht, Nadav Bandel, Gassan Moady, Monah Shehadeh, Tali Reuveni, et al., The impact of empagliflozin on cardiac physiology and fibrosis early after myocardial infarction in non-diabetic rats, Cardiovasc. Diabetol. 20 (1) (2021 Jul 2) 132, https://doi.org/10.1186/s12933-021-01322-6.

[18] M. Li, K.C.K. Lloyd, DNA fragmentation index (DFI) as a measure of sperm quality and fertility in mice, Sci. Rep. 10 (1) (2020 Mar 2) 3833, https://doi.org/10.1186/10.1038/s41598-020-60876-9.

[19] Tao Tian, Ke-Jun Nan, Shu-Hong Wang, Xuan Liang, Chuang-Xin Lu, Hui Guo, et al., PTEN regulates angiogenesis and VEGF expression through phosphatase dependent and -independent mechanisms in HepG2 cells, Carcinogenesis 31 (7) (2010) 1211–1219, https://doi.org/10.1093/carcin/bgq085.

[20] Paaladinesh Thavendiranathan, Bernd J. Wintersperger, D. Scott, Flamm, Thomas H. Marwick, Cardiac, Cardiac MRI in the assessment of cardiac injury and toxicity from cancer chemotherapy: a systematic review, Circulation: Cardiovasc Imaging 6 (6) (2013 Nov) 1080–1091, https://doi.org/10.1161/CIRCIMAGING.113.000899.

[21] Emma Louise Robinson, Maral Azodi, Stephane Heymans, Heggermont Ward, et al., Anthracycline-related heart failure: certain knowledge and open questions : where do we stand with chemotherapyinduced cardiotoxicity? Curr. Heart Fail. Rep. 17 (6) (2020) 357–364, https://doi.org/10.1161/10.1007/s11897-020-00489-5.

[22] Laura C. Saunders, Chris S. Johns, Neil J. Stewart, Charlotte J.E. Oram, David A. Capener, O. Valentina, Puntmann, et al., Diagnostic and prognostic significance of cardiovascular magnetic resonance native myocardial T1 mapping in patients with pulmonary hypertension, J. Cardiovasc. Magn. Reson. 20 (1) (2018) 78, https://doi.org/10.1186/s12968-018-0501-8. Dec 3.

[23] Hoshang Farhad, V. Pedro, Staziaki, Daniel Addison, Otavio R. Coelho-Filho, Ravi V. Shah, Richard N. Mitchell, et al., Characterization of the changes in cardiac structure and function in mice treated with anthracyclines using serial cardiac magnetic resonance imaging, Circulation: Cardiovascular Imaging 9 (12) (2016 Dec), e003584, https://doi.org/10.1161/CIRCIMAGING.115.003584.

[24] Julian A. Luetkens, Marilia Voigt, Anton Faron, Isaak Alexander, Narine Mesropyan, Darius Dabir, M. Alois, Sprinkart, et al., Influence of hydration status on cardiovascular magnetic resonance myocardial T1 and T2 relaxation time assessment: an intraindividual study in healthy subjects, J. Cardiovasc. Magn. Reson. 22 (1) (2020 Sep 7) 63, https://doi.org/10.1186/s12968-020-00661-9.

[25] Yoo Jin, Hong, Heae Surng Park, Jeffrey Kihyun Park, Kyunghwa Han, Chul Hwan Park, Tai Kyung Kim, et al., Early detection and serial monitoring of AnthracyclineInduced cardiotoxicity using T1-mapping cardiac magnetic resonance imaging: an animal study, Sci. Rep. 7 (1) (2017 Jun 1) 2663, https://doi.org/10.1038/s41598-017-02627-x.

[26] Enver Tahir, Manuella Azar, Sahar Shihada, Katharina Seiffert, Yvonne Goy, Antonia Beitzen-Heineke, et al., Myocardial injury detected by T1 and T2 mapping on CMR predicts subsequent cancer therapy–related cardiac dysfunction in patients with breast cancer treated by epirubicin-based chemotherapy or left-sided RT, Eur. Radiol. 32 (3) (2022) 1853–1865, https://doi.org/10.1007/s00330-021-08260-7.

[27] Saule Balmagambetova, Zhenisgul Tlegenova, Bekbolat Zholdin, Gulnara Kurmanalina, Iliada Talipova, Arip Koyshybaev, et al., Early diagnosis of chemotherapy-linked cardiotoxicity in breast cancer patients using conventional biomarker panel: a prospective study protocol, Diagnostics 12 (11) (2022) 2714, https://doi.org/10.3390/diagnostics12112714. Nov 6.

[28] Carlos Galán-Arriola, Jean Paul Vílchez-Tschischke, Manuel Lobo, López Gonzalo J, Antonio de Molina-Iracheta, Claudia Pérez-Martínez, et al., Coronary microcirculation damage in anthracycline cardiotoxicity, Cardiovasc. Res. 118 (2) (2022) 531–541, https://doi.org/10.1093/cvr/cvab053.